ABSTRACT

Contour Extraction From HVEM Image of Microvessel
Using Active Contour Models

by
Manping Xiao

This thesis reports the research results on automatic contour extraction from high voltage electron microscope (HVEM) image of thick cross section montages of small blood vessels. The previous work on this subject, which was based on the conventional edge detection operations combined with edge linking, has proven inadequate to describe the inner structural compartments of microvessels. In this thesis, an active contour model (commonly referred to as "Snakes") has been applied to advance the previous work. Active contour models have proven themselves to be a powerful and flexible paradigm for many problems in image understanding, especially in contour extraction from medical images. With the developed energy functions, the active contour is attracted towards the edges under the action of internal forces (describing some elasticity properties of the contour), image forces and external forces by means of minimization of the energy functions. Based on this active model, an effective algorithm is implemented as a powerful tool for 2-D contour extraction in our problem for the first time. The results thus obtained turn out to be encouraging.

CONTOUR EXTRACTION FROM HVEM IMAGE OF MICROVESSEL USING ACTIVE CONTOUR MODELS

by
Manping Xiao

A Thesis
Submitted to the Faculty of
New Jersey Institute of Technology
in Partial Fulfillment of the Requirements for the Degree of
Master of Science in Biomedical Engineering

Biomedical Engineering Committee

January 1994

Contour Extraction From HVEM Image of Microvessel
Using Active Contour Models

Manping Xiao

| Dr. Yun-Qing Shi, Thesis Advisor | Date |
| Assistant Professor of Electrical Engineering, NJIT | |

Dr. David Kristol, Committee Member	Date
Professor of Chemistry, Director and Graduate	
Advisor of Biomedical Engineering , NJIT	

Dr. L. Horn, Committee Member	Date
Professor of Physiology, University of	
Medicine and Dentistry of New Jersey.	

BIOGRAPHICAL SKETCH

Author: Manping Xiao

Degree: Master of Science in Biomedical Engineering

Date: January 1994

Graduate and Undergraduate Education:

- Master of Science in Biomedical Engineering
  New Jersey Institute of Technology, Newark, NJ, 1994

- Bachelor of Science in Biomedical Engineering
  Zhejiang University, Hangzhou, P. R. China

Major: Biomedical Engineering

This thesis is dedicated to my dear parents

ACKNOWLEDGMENT

I wish to express my sincere gratitude to my thesis advisor, Dr. Yun Q. Shi, for his guidance, friendship, encouragement and support throughout this research. I am specially indebted to him for his insightful and constructive criticisms at every stage of this thesis.

I would like to express my deep appreciation to Dr. David Kristol for his encouragement, kindness and financial support during this research and also for his guidance in my whole graduate program and serving as a member of the committee.

Special thanks to Professor L. Horn for his recognition of the problem in the field of microcirculation which is very helpful in this thesis. I appreciate his providing me with the HVEM pictures and serving as a member of the committee.

I appreciate the timely help from Guang Yang, Kuen Tak Wong, Xiaojin Deng and the computer consultants at UMDNJ who provided me important computer system information. This work could not be completed without this help.

TABLE OF CONTENTS

LIST OF FIGURES

CHAPTER 1

INTRODUCTION

1.1 Research Background

Every cell and every organ system in the body depend upon the circulation of blood for appropriate nutrients, humoral message exchange and removal of waste [1]. The smallest arteries, arterioles, capillaries and venules are generally considered the key vessels, the first two types mediating the distribution of the flow by changing their diameters and thus flow resistance and the latter two being the most important for their fluid and solute exchange properties. The structural aspects of these vessels therefore become crucial for the understanding of the mechanism that allow the optimal harmony for good health.

Substantial advances have been made in the knowledge of the microcirculation particularly within the last thirty years. A combination of innovative methods and technology have made it possible to describe microvascular behavior in more precise quantitative terms. Microtechniques and computer assisted analysis of intra vital video microscopy have enabled us to study individual segments of the microcirculation vessel system for more accurate analysis and use such information to reconstruct the operational characteristics of an entire microvascular bed [2].

The most recent combination of the high voltage electron microscope (HVEM) and powerful computers allows to digitize microvascular electron microscope images and display them directly on the monitor along with the associated contour lines [1]. A three dimensional reconstructed picture is generated by using a series of sequential microscopic images simultaneously.

1

This provides a method for assessment of detailed structure of microvessels. Such a method can also be amenable to both numerical calculations of parameters of cell wall compartments and can be used for image reconstruction of the vessel in solid or transparent mode that can be viewed from any chosen angle and can allow for computerized dissection.

In this method, image recognition of the vessel in solid and transparent mode and computerized dissection of cell compartments are performed by using the contour data of the cross-section of microvessels. Thus, to provide a method, that will devise an accurate, versatile and time saving assessment of the detailed description of the contours of microvascular vessels, becomes very important.

1.2 Active Contour Model

Extracting boundaries (or contour) of objects from noisy images is an important problem in computer vision and image processing, especially in medical image processing applications. Traditional segmentation approaches have proven inadequate when faced with anatomical complexity and variability exhibited by biological structures [3]. Traditional approaches to finding object boundaries involve some form of local, low-level feature detection in order to locate image gradients. The gradients information is then used to interpret an object contour or surface. Unfortunately, noise and image artifacts can cause discontinuities to appear in boundaries recovered by these methods [4].

Recently Kass et al. have proposed a model called active contour (Snakes) which has the advantage that the final form of a contour can be influenced by feedback from a higher level process [4]. This model is an energy-minimization scheme based on the assumption that object boundaries

are continuous and smooth. The idea behind active contours is to redefine certain computer vision problems in terms of energy-minimization, a problem which has been thoroughly developed in the mathematical literature. The contour is initially placed near an edge under consideration, then image forces or external forces draw the contour to the edge of the image. As the algorithm iterates, the energy terms can be adjusted by higher level processes to obtain a global minimum. This method of redefining problems in terms of energy minimization makes active contours a very flexible tool with a variety of adaptations to solve particular problems. Snakes, or active contour models, are energy-minimizing splines which can be used to find image features such as minima or edges, and can be subject to a variety of user-defined, externally-generated "forces" in order to assist the snakes in finding the solution to the minimization problem.

Active contour models have been applied to certain medical image understanding problems. Cohen introduced a "balloon-expansion" force inside a closed contour model to find the endocardial wall in transverse magnetic resonance images of the heart [5]. Rong applied active contour models to the detection of coronary arteries in digital subtraction angiography images of the beating heart [6]. Gwydir et al. used continuity splines to analyze neurite outgrowth and growth cone motility [7]. In this thesis, an active contour model is used to extract contours of microvessels from HVEM images. The results are encouraging.

Research in active contour models has primarily focused on the methods of solving the variational problem, while illustrating these methods with a particular application. Kass, Witkin, and Terzopoulos solved the variational problem by employing Euler-Lagrange equations from calculus of variations [4]. The Euler-Lagrange equations result in partial differential

equations which the above authors solved by using the finite difference method. Cohen and Cohen also employed calculus of variations, but used the Galerkin solution from the finite element method to solve the Euler-Lagrange equations [8]. Recently, Amini showed that dynamic programming could be used to solve many variational problems in computer vision, including the problem of energy-minimizing active contour models [9]. Williams and Shah proposed an active contour model using greedy algorithms, which is more stable and approaches minimum energy rapidly without costly matrix calculations [10]. This method works well when there is a prior knowledge of the data, as in our case. For each iteration of the program, a snake point can move to a set of its neighboring points, or remain at the same point, depending on which of the set of points has the minimum energy.

My research work reported in this thesis employs Snakes to extract contours from HVEM image of microvessel instead of traditional methods of contour detection and develops an algorithm to implement the Snakes model.

CHAPTER 2

PROBLEM BACKGROUND

2.1 Basic Structure of Microvessel

The specimen of a microvessel is composed of vascular smooth muscle (VSM), internal lamina (IL), endothelium (EN), vascular smooth muscle nucleus (VSM-NUC), endothelium nucleus (EN-NUC), and lumen (L) which are shown in Figure 2.1. These elements or compartments used frequently in the following chapters are the objects of interest that play an important role in the microcirculation. The changes in their shape and size provide information for the microcirculation research.

2.2 Contour Data Acquisition

2.2.1 Conventional Manual Method

There are two steps in collecting the boundary or contour data from the final glossy prints in this method [1].

1) Mark compartment contours on a clear plastic overlay;

2) Convert those marked curves into data files. This work is accomplished by hand. A full-sized transparent overlay is placed over the microvessel electronmicrograph print. An investigator uses a water colored pen to trace the contour of particular compartment from a knowledge of the microvessel. One color is assigned to one particular compartment to obtain cross section contours. Then the marked plastic overlay is placed on a digitizing tablet called Digipad with fixed x-y coordinate. An operator holds a probe, that is connected to the digitizer interface, to follow each marked close contour. The coordinates of every point along the contour are
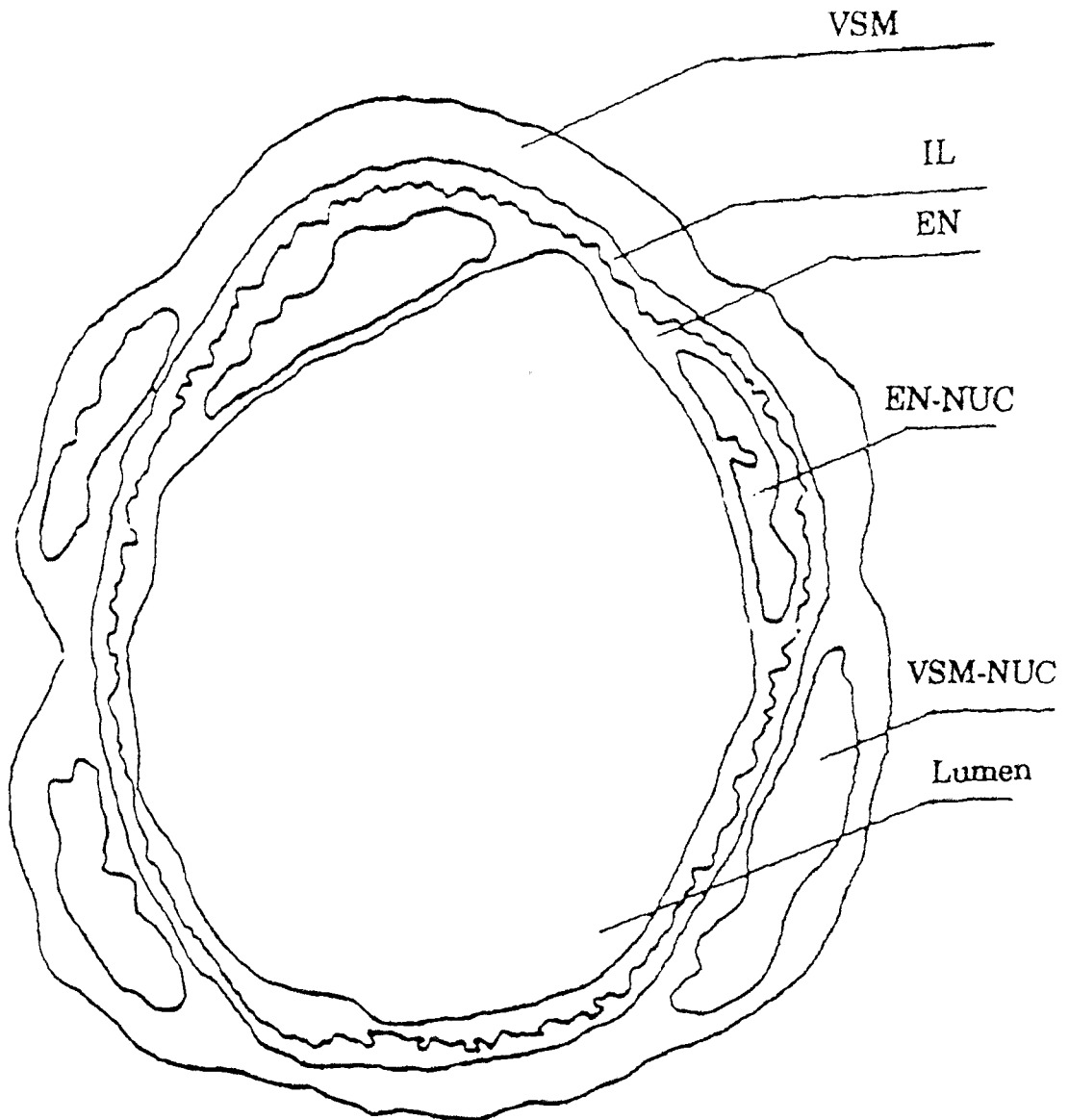
5

Figure 2.1 Basic Structure of Microvessels
Key: VSM -- Vascular Smooth Muscle
      IL -- Internal Lamina
      EN -- Endothelium
      VSM-NUC--Vasc. Smooth Muscle Nucleus
      EN-NUC--Endothelium Nucleus

transformed into data. Then data are collected by the computer and stored as a data file.

This manual data acquisition is a time consuming and tedious job. It is a routine job in processing the experimental microvessel specimen. An automatic digital image data acquisition system is demanded by the researchers in their study of HVEM image of microvessels.

2.2.2 Method of Conventional Digital Image Processing

A synthetic method of automatic contour extraction from HVEM images of microvessels was proposed by Liu et al. [11]. The method consists of several computer image processing techniques including median and extreme transforms, edge detection, edge linking and edge thinning. It is tested on the HVEM images of thick cross sections of microvessels. A gray scaled HVEM image is transferred into a binary code one pixel thick boundary picture, and a corresponding coordinate data file is created at the same time. The data file could serve as input to a 3-D image reconstruction device.

This can be considered as a traditional approach to boundary detection. Objects in images are defined by their boundaries, which usually appear as abrupt changes in image intensity. After gradients of images are computed, the maxima of image intensity changes are extracted and then edges are linked together. Traditional approaches to finding object boundaries involve some form of local, low-level feature detection in order to locate these image gradients. The gradient information is then used to interpret object contours.

Figure 2.2 shows the result obtained by using this digital image processing method. The results demonstrate that it is possible to use computer image processing techniques instead of manual methods to obtain contour data from electronmicroscopic pictures. However, it is also obvious

that information of small compartments of the microvessels such as IL, EN and VN are missing after application of this method.
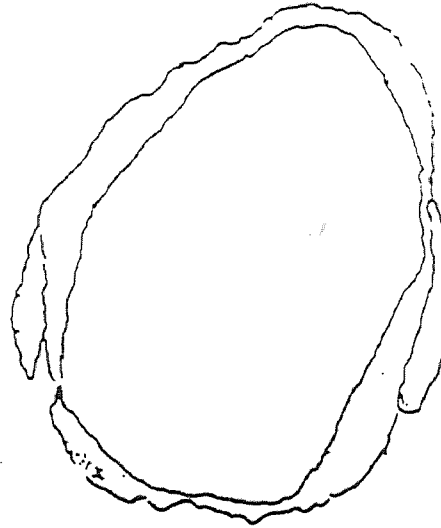
Figure 2.2 Final one pixel thick boundary picture in Liu's method

In real-world images especially medical images, object boundaries cannot be detected solely on the basis of their photometry because of the presence of noise and various photometry anomalies . Thus, all methods for finding boundaries based on purely local statistical criteria are bound to generate errors, finding either too many or too few edges, because they lack a geometrical model to guide their search. Based on these problems, Kass et al. presented a technique that integrates both photometry and geometric models with an initial estimate of the boundary [4]. The models are incorporated by defining an energy function for curves that is minimal when the models are exactly satisfied. The initial estimate is used as the starting points for finding a local minimum of this energy function by embedding the initial curve in a

viscous medium and solving the equations of dynamics. The strength of this "energy-minimizing curve" approach are that the geometric constraints are directly used to guide the search for a boundary and that the edge information is integrated along the entire length of the curve, thereby providing a large support without including the irrelevant information off of the curve and at the same time finding boundaries that could not otherwise be found. This kind of geometric model is what are called active contour models, also called Snakes because of the way the contours slither while minimizing their energy.

CHAPTER 3

ACTIVE CONTOUR MODEL

3.1 Basic Snake Behavior

The basic Snake model is a controlled continuity spline under the influence of image forces and external constraint forces [4]. The internal spline forces serve to impose a piecewise smoothness constraint. The image forces push the Snake toward salient image features such as lines and edges. The external constraint forces are responsible for placing the Snake near the desired local minimum. These forces can, for example, come from a user interface, automatic attentional mechanisms, or high-level interpretations.

3.2 Mathematical Description of Snakes

In their work, Kass et al. represented a contour by a vector $v(s) = [x(s) \ y(s)]^T$, having the arc length, s, as a parameter [4]. They defined an energy functional of the contour and described a method for finding contours which correspond to local minima of the functional. The energy functional is written as

$$E^* = \int_0^1 E(v)ds$$
$$= \int_0^1 (E_{int}(v) + E_{image}(v) + E_{ext}(v))ds. \qquad (3.1)$$

where $E(v)$ is defined as the overall energy:

$$E(v) = E_{int}(v) + E_{image}(v) + E_{ext}(v) \qquad (3.2)$$

10

E_{int} represents the internal energy of the contour due to bending or discontinuities, E_{image} is the image forces, and E_{ext} is the external forces.

The internal energy, sometimes also referred to as the spline energy, is written as

$$E_{spline}(v(s)) = E_{int}(v(s))$$
$$= \alpha(s) |v_s(s)|^2 + \beta(s) |v_{ss}(s)|^2 \tag{3.3}$$

where $\alpha(s)$ and $\beta(s)$ are functions that control the elasticity and rigidity of the spline, respectively. The terms $v_s(s)$ and $v_{ss}(s)$ are the first and second order derivatives of $v(s)$ with respect to s, respectively.

The above equation contains a first-order term which will have large values where there is a gap in the curve, and a second-order term which will be larger where the curve is bending rapidly. The values of α and β at a point determine the extent to which the contour is allowed to stretch or bend at that point. The relative sizes of α and β can be chosen to control the influence of the corresponding constraints. For instance, a large value of β would make the second-order term larger than the other term; thus the minimum value of E^* would occur when the curve was smoother, approaching a circle for a closed contour, and a straight line for a contour which was not closed. If α is 0 at a point, a discontinuity can occur at that point, while if β is 0, a corner can develop, because large values of these terms would not be included in the total.

From calculus, we know that the length of a parametrically-defined planar curve $v(s)=(x(s),y(s))$ where $0 \le s \le 1$ (normalized) is

$$L = \int_0^1 \sqrt{\left(\frac{dx(s)}{ds}\right)^2 + \left(\frac{dy(s)}{ds}\right)^2} \qquad (3.4)$$

Also note that the term $|v_s|^2$ from equation 1 can be written as

$$|V_s|^2 = \left(\frac{dx(s)}{ds}\right)^2 + \left(\frac{dy(s)}{ds}\right)^2 \qquad (3.5)$$

Therefore, the above equations state that the overall length of the spline can be obtained by integrating $|v_s|$ over the entire length of the spline. Notice also that $|V_s|$ is the magnitude of the vector which is tangent to $|V_s|$. From the above observations, we can then make several conclusions concerning the elasticity-controlling function $\alpha(s)$:

1. If $\alpha(s) > 0$ in a particular region, then the minimization process will tend to minimize the length of the spline in that region, producing a contraction effect.

2. If $\alpha(s) = 0$ in a region, then the length of the spline should not be affected.

3. If $\alpha(s) < 0$, the system diverges.

4. The normal minimization process will tend to minimize the magnitude of the tangential vector, thereby forcing the spline to tend toward a straight line.

Similar comments can be made for the effect of $\beta(s)$, the flexibility-controlling term. Since $\beta(s)$ operates on a second derivative term, it will affect the degree to which the spline is "straightened out" and where the straightening occurs. Allowing $\beta(s)$ to go to zero at a particular s would allow the magnitude of the second derivative of $v(s)$ to be arbitrarily large at that point-thus allowing for a discontinuity at that point. However, a large value of $\beta(s)$ would make the second-order term larger than the other term; thus the minimum value of $E(v)$ would occur when the curve was smoother, approaching a circle for a circle for a closed contour, and a straight line for a contour which was not closed. In this particular application, we assume that the microvessels are relatively smooth and do not have sharp corners or discontinuities.

An additional energy functional $E_{image}(v)$ is defined which includes the influence of the image. It is used to generate gradients to push or pull the Snake in a particular direction. The image forces can be determined by to various events. Those presented by Kass et al. are lines and edges. If

$$E_{image}(x,y) = kI(x,y) \tag{3.6}$$

where $I(x,y)$ is the image intensity function, then the Snake will tend toward ridges or valleys in the image, depending upon the sign of k. If

$$E_{image} = -|\nabla I(x,y)|^2 \tag{3.7}$$

where $\nabla I(x,y)$ is the gradient of the image, then the Snake will tend toward edges in the image. The overall E_{image} can be written as:

$$E_{image}(x,y) = W_{image} I(x,y) + W_{edge} |\nabla I(x,y)|^2 \qquad (3.8)$$

where W_{image} and W_{edge} are relative weights in the range [-1,-1].

E_{ext} is used to denote the energy function of external constraint forces which are responsible for putting the Snake near the desired local minimum. For example, an energy function E_{magnet} can be defined which will repulse or attract the snake in a particular direction[6], depending upon the sign of k_{magnet} (constant). Also, an energy function E_{spring} can be defined which always pulls the snake toward a particular (x,y) location. We shall let

$$E_{magnet}(x,y) = \frac{k_{magnet}}{(x-x_{magnet})^2 + (y-y_{magnet})^2} \qquad (3.9)$$

and let

$$E_{spring}(x,y) = k_{spring}((x - x_{spring})^2 + (y - y_{spring})^2). \qquad (3.10)$$

Therefore, the overall E_{ext} can be written as

$$E_{ext}(x,y) = W_{magnet}E_{magnet}(x,y) + W_{spring}E_{spring}. \qquad (3.11)$$

where W_{magnet} and W_{spring} are relative weights in the range [-1,1].

The Euler-Lagrange condition from the calculus of variations states that the spline $v(s)$ which minimizes E^* must satisfy

$$\frac{d}{ds}E_{vs} - E_v = 0 \qquad (3.12)$$

where Ev_s is the partial derivative of E with respect to v_s and Ev is the partial derivative of E with respect to v. The above equation reduces to

$$-\frac{d}{ds}(\alpha(s)v_s(s)) + \frac{d^2}{ds^2}(\beta(s)v_{ss}(s)) + \nabla E_{image}(v(s)) + \nabla E_{ext}(v(s)) = 0 \quad (3.13)$$

In order to solve the Euler-Lagrange equation, we assume that we have an initial estimate of $v(s)$ and then have an evolution equation

$$\frac{\partial v(s,t)}{\partial t} - \frac{\partial}{\partial s}(\alpha(s)\frac{\partial v(s,t)}{\partial s}) + \frac{\partial^2}{\partial s^2}(\beta(s)\frac{\partial v^2(s,t)}{\partial s^2}) + \nabla E_{image}(v(s)) + \nabla E_{ext}(v(s,t)) = 0$$

$$(3.14)$$

so that when $\frac{\partial v(s,t)}{\partial t}$ goes to zero, then a solution to Euler-Lagrange equation has been found.

At this point, a few different numerical solutions have been developed. Kass et al. estimated the partial derivatives in s and t by the finite differences method, which is by far the simplest solution, but several inherent problems of numerical instability must be avoided [4]. Cohen and Cohen used the Galerkin solution of the finite element method which has the advantage of greater numerical stability and better efficiency than the method Kass et al. proposed [8]. However, there are some problems with both of these solutions. Williams et al. pointed out some of these, including instability and a tendency for points to bunch up on a strong portion of an edge [10]. They have proposed a greedy algorithm for minimizing the energy functional to obtain more desirable behavior of the Snakes.

The following is a description of the most basic and original solution of the Snakes model developed by Kass et al. [4].

When $\alpha(s)=a$, and $\beta(s)=b$ are constants, minimizing the energy functional of equation (3.1) gives rise to the following two independent Euler-Lagrange equations:

$$\alpha x_{ss} + \beta x_{ssss} + \frac{\partial E_{image}}{\partial x} + \frac{\partial E_{ext}}{\partial x} = 0 \tag{3.15}$$

$$\alpha y_{ss} + \beta y_{ssss} + \frac{\partial E_{image}}{\partial x} + \frac{\partial E_{ext}}{\partial y} = 0 \tag{3.16}$$

where x_{ss} and x_{ssss} are the second and fourth order derivatives of x with respect to s, respectively, y_{ss} and y_{ssss} are the second and fourth order derivatives of y with respect to s, respectively.

When $\alpha(s)$ and $\beta(s)$ are not constant, it is simpler to go directly to a discrete formulation of the energy functional in equation (3.1), that is

$$E_{snake} = \sum_{i=1}^{n}(E_{int}(i) + E_{image}(i) + E_{ext}(i)) \tag{3.17}$$

Approximating the derivatives with finite differences and converting to vector notation with $v_i=(x_i,y_i)=(x(ih),y(ih))$, we expand $E_{int}(i)$

$$E_{int}(i) = \alpha_i|v_i - v_{i-1}|^2 / 2h^2 + \beta_i|v_{i-1} - 2v_i + v_{i+1}|^2 / 2h^4 \tag{3.18}$$

where we define $v(0)=v(n)$, h is the unit length in the second derivative. Let

$$f_x(i) = \partial E_{image}/\partial x_i + \partial E_{ext}/\partial x_i$$

and

$$f_y(i) = \partial E_{image}/\partial y_i + \partial E_{ext}/\partial y_i$$

where the derivatives are approximated by a finite difference if they cannot be computed analytically. Now the corresponding Euler-Lagrange equations are

$$\alpha_i(v_i - v_{i-1}) - \beta_{i+1}(v_{i+1} - v_i) + \beta_{i-1}[v_{i-2} - 2v_{i-1} + v_i]$$
$$- 2\beta_i[v_{i-1} - 2v_i + v_{i+1}] + \beta_{i+1}[v_i - 2v_{i+1} + v_{i+2}]$$
$$+ (f_x(i), f_y(i)) = 0 \qquad (3.19)$$

The above Euler equations can be written in matrix form as:

$$Ax + f_x(x,y) = 0 \qquad (3.20)$$
$$Ay + f_y(x,y) = 0 \qquad (3.21)$$

where A is a pentadiagonal banded matrix.

To solve Equation (3.20) and (3.21), we set the right-hand sides of the equations equal to the product of a step size and the negative time derivatives of a step size of the left-hand sides. Taking into account derivatives of the external forces we use requires changing A at each iteration, so we achieve faster iteration by simply assuming that f_x and f_y are constant during a time step. This yields an explicit Euler method with respect to the external forces. The internal forces, however, are completely specified by the banded matrix, so we can evaluate the time derivative at time t rather than time t-1 and

therefore arrive at an implicit Euler step for the internal forces. The resulting equations are

$$Ax_t + f_x(x_{t-1}, y_{t-1}) = -g(x_t - x_{t-1}) \tag{3.22}$$

$$Ay_t + f_y(x_{t-1}, y_{t-1}) = -g(y_t - y_{t-1}) \tag{3.23}$$

where g is a step size. At equilibrium, the time derivative vanishes and we end up with a solution of Equations (3.20) and (3.21).

Equations (3.22) and (3.23) can be solved by matrix inversion:

$$x_t = (A + gI)(x_{t-1} - f_x(x_{t-1}, y_{t-1})) \tag{3.24}$$

$$y_t = (A + gI)(y_{t-1} - f_y(x_{t-1}, y_{t-1})) \tag{3.25}$$

The matrix $A+gI$ is a pentadiagonal banded matrix, so its inverse can calculated by LU decompositions in $O(n)$ time. Hence Equation (3.24) and (3.25) provide a rapid solution to Equation (3.20) and (3.21). The method is implicit with respect to the internal forces, therefore it can solve very rigid Snakes with large step sizes. If the external forces become large, however, the explicit Euler steps of the external forces will require much smaller step sizes.

CHAPTER 4

IMPLEMENTATION OF SNAKES AND ALGORITHM

4.1 Digitized Image

Before any processing can be implemented, enlarged HVEM prints must be converted into digitized images that are acceptable by a computer. There are several kinds of image digitization devices. For example, scanners, video cameras, even fax machines can be used.

In my research, I used a scanner (Hewlett Packard ScanJet IIc model), a Macintosh computer and a SUN workstation to digitize enlarged HVEM prints which were obtained from Dr. L. Horn from his work with the HVEM group at the Wadsworth Center for Laboratories and Research at New York State Department of Health. The HP scanner is connected to a Macintosh computer. After scanning, a 670x350 8-bit gray TIFF(Tag Image File Format) format computer file is formed from HVEM prints.

Then the TIFF file is transferred from the Macintosh to the SUN workstation. The TIFF data is converted by using the specific conversion program into a VIFF file, a format that is compatible with the software called KHOROS assembled in the SUN workstation at NJIT. The purpose is to use SUN workstations as computing platforms, that have a high resolution monitor, and to use KHOROS as a library of software that can provide capability for sophisticated image processing and visualization. Figure 4.1 shows the gray level scaled original image that is a part of a cross-section of digitized HVEM microvessel image.

Figure 4.1 Gray level scaled original image

4.2 Pre-processing

The first task is the pre-processing which makes subsequent processing easier and accurately.

The task of pre-processing is to eliminate the surrounding useless parts of the microvessel in the image because the response from these useless parts may interfere with the extraction of microvessel boundaries.

This part of the program is developed in the CANTATA, which is a visual programming environment in the SUN workstation for the rapid prototyping of information processing programs based on the KHOROS library of routines [12]. At first, cutting the unwanted regions using the cutting program, a relatively "clean" image is generated, see Figure 4.2. After cutting, image preprocessing included speckle reduction and image smoothing.

4.2.1 Speckle Reduction

It is desirable to reduce speckle noise in raw images for late usage of automatic recognition algorithms on computer. The goal is to smooth out the speckle but at the same time preserve features of interest such as the arteriole ring as in our case.

A nonlinear geometric filter, based upon geometric concepts, was used to accomplished this [13]. This filter uses the complementary hulling technique to reduce the speckle index of an image. The algorithm is available in KHOROS routine library. It is an iterative algorithm which usually requires about ten iterations to reach an optimal effect [12].

The geometric filter utilizes the complementary technique which has a history starting with a problem which has nothing to do with speckle reduction [13]. The original problem was to generate approximations of the
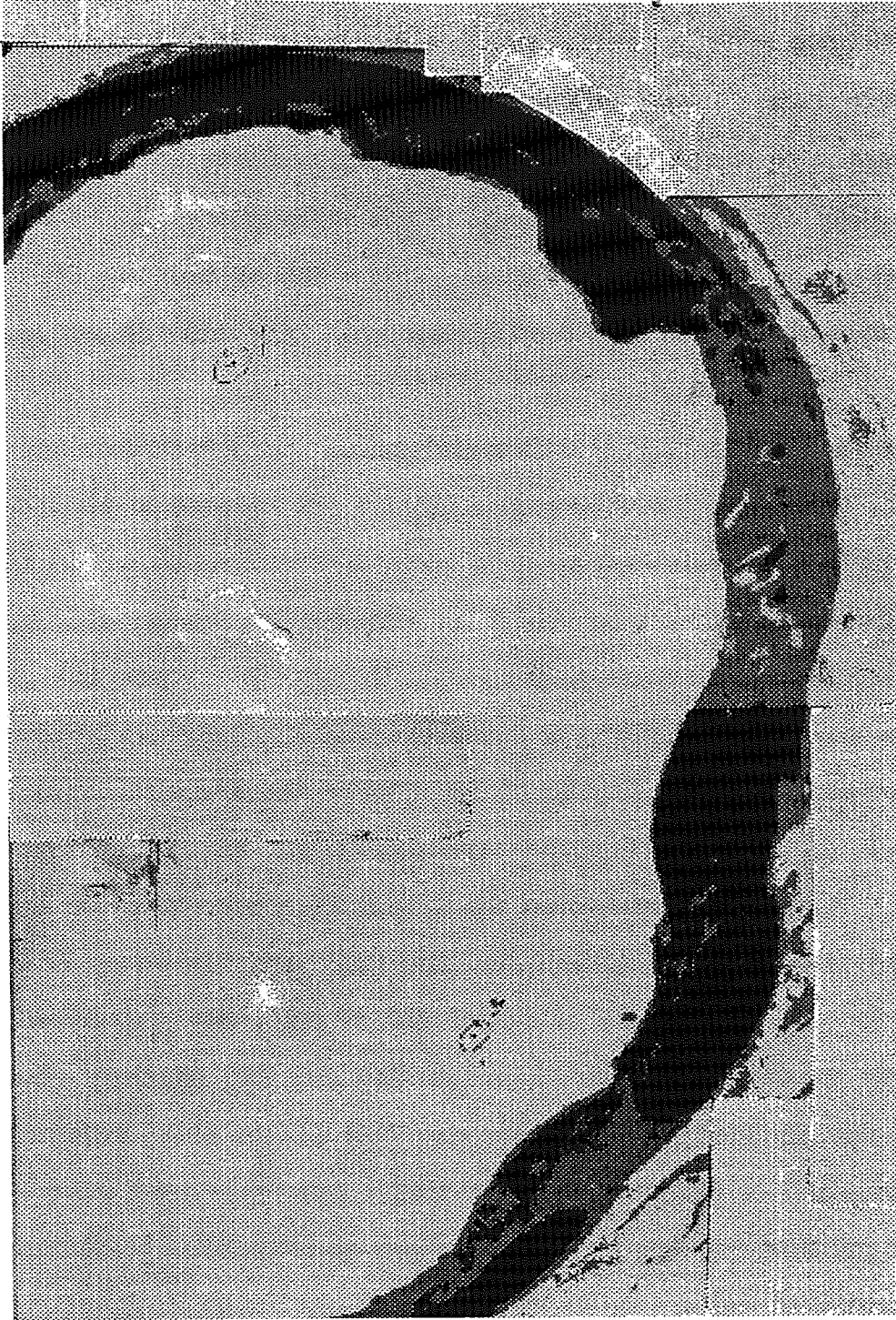
Figure 4.2 Gray level scaled image after cutting

convex hulls of maximal connected subsets of foreground of a binary image. (The foreground is the set of pixels with values 1.) The motivation for this was enhancement of medical imagery. The convex hull of a set is the intersection of all the half-planes containing it. An approximation to this, calles the 8-hull, is defined as the intersection of only those half-planes which contain the set and whose edges are either horizontal or vertical or lie in either of the 45^0 diagonal directions. The 8-hull of a set has, at most, eight sides.

The complementary hulling algorithm is an iterative algorithm [13]. It is developed to smooth the ragged edges of binary images. One iteration consists of the following. First, one step of the 8-hull algorithm, that is an iterative algorithm to generate an 8 hull of a set, is applied to the set. Second, one step of the 8-hull algorithm is applied to its complement. In other words, one step of 8-hull algorithm is applied, then zeros and ones are interchanged, then another step of the 8-hull algorithm is applied, and finally, zeros and ones are interchanged again. This has an effect of gradually reducing the maximum curvature of the boundary of the set.

The geometric filter uses this complementary hulling technique in the following way. Each pixel in the image is compared with all eight of its surrounding pixels. The pixels above and below the pixel are the N-S pair, the pixels on either side are the E-W pair, those on diagonals are the NW-SE and NE-SW pair. The image and a pair of pixels are sent to the symmetric hull function which in turn sends the image to the positive hull function and to the negative hull function. The positive and negative hull functions are called twice; the first time the neighboring pair of pixels is sent and the second time the complement of the pixels is sent. The positive hull function replaces each "middle pixel" with the result of a several comparisons. These

comparisons are a combination of maximums and minimums. The final comparison is a maximum for the positive hull algorithm. The image is then sent to the negative hull function where the middle pixel is replaced with the result of more comparisons. The final comparison for the negative hull algorithm is a minimum. The result of all these replacements has the effect of reducing the undesired speckle noise while preserving the edges of the original image. We can see this result in Figure 4.3.

4.2.2 Image Smoothing

To use the active contour models, we have to estimate the initial contours that are chosen to be placed near an edge under consideration. For this purpose, we can count on conventional local edge detection techniques. The edges coincide, generally speaking, with gray level transition, so they can be detected by gradients or the zero-crossing of the second order derivatives calculated by some differential operators [12]. Because the differential operators are sensitive to noise, a preprocessing such as smoothing is often necessary to eliminate the noise. One well-known smoothing filter is the Gaussian filter and the edges can therefore be detected by a Laplacien-Gaussian filter. The edges can therefore be detected by using a Laplacien-Gaussian filter. But there is an essential difficulty in applying the Laplacien-Gaussian filter that is the conflict between the smoothing effect and the precision of edge localization. To overcome this difficulty, Castan proposed an optimal exponential filter based on one step model (a step edge and white noise) and multi-edge model [12]. This optimal smoothing filter is a symmetric exponential filter of an infinitely large window size and can be realized by a very simple recursive algorithm in the KHOROS library of routines.
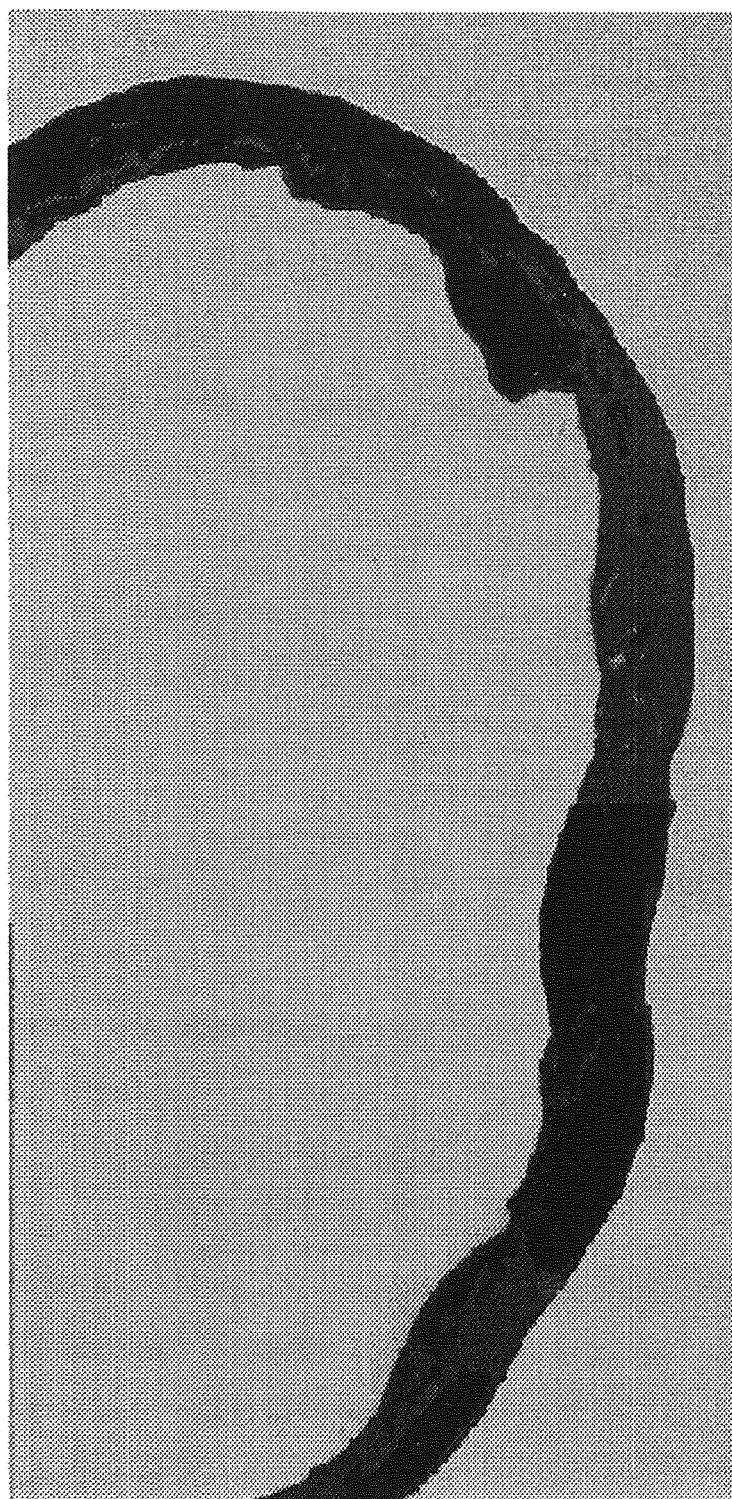
Figure 4.3 Gray level scaled image after speckle reduction

A normalized symmetric exponential filter on 1-D can be written as:

$$fL(x) = ca_0(1 - a_0)^{|x|} = f_1(x) \# f_2(x)$$

$$= c(f_1(x) + f_2(x) - a_0 d(x)) \tag{4.1}$$

where:

a_0 is the filter parameter, $c = 1/(2-a_0)$

\# means the convolution, $d(x)$ is dirac function.

$$f_1(x) = \begin{cases} 0 & \text{if} \quad x < 0 \\ a_0(1-a_0)^x & \text{if} \quad x \geq 0 \end{cases} \tag{4.2}$$

$$f_2(x) = \begin{cases} a_0(1-a_0)^{-x} & \text{if} \quad x \leq 0 \\ 0 & \text{if} \quad x > 0 \end{cases} \tag{4.3}$$

Because the exponential function is separable, we can write out 2-D exponential filter:

$$f(x,y) = fL(x) * fL(y) \tag{4.4}$$

Figure 4.4 shows the image after smoothing by this optimal exponential filter and we see the exponential filter has the very obvious noise eliminating effect. It is shown in the following section that the symmetric exponential filter is also the optimal edge detector filter in the criteria of the signal to noise ratio, the localization precision and antique maximum. We can see this result in Figure 4.5.
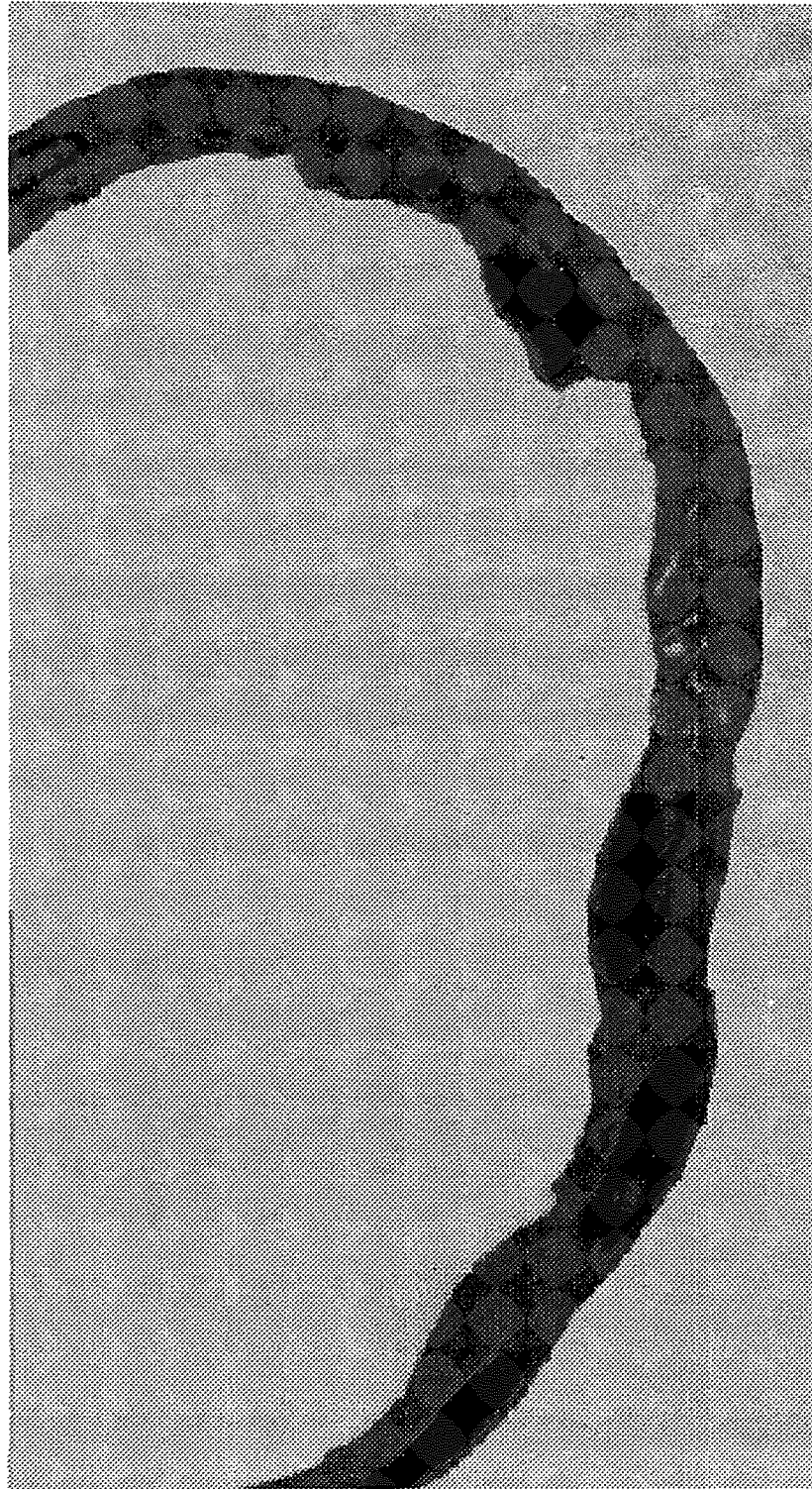
Figure 4.4 Gray level scaled image after smoothing

4.3 Implementation of Snakes

4.3.1 Initial Contour Estimation

As discussed above, we must give an initial contour estimation before using the Snakes according to Williams's algorithm [10]. The initial contour of the microvessel in my research was produced by the edge detection algorithm developed by Castan [12]. This allows us to combine the quality of a good local edge detector with global active model.

The Castan edge detector is based on the symmetric exponential filter of an infinitely large window size, that is discussed in Section 4.2.2. According to Castan, the band-limited first and second directional derivative of the input image filtered by the symmetric exponential filter can be obtained by the algorithms as stated below. Using them, then the edge detection for an image can be realized.

We can write the first order derivative operator of exponential filter:

$$fL'(x) = f_2(x) - f_1(x) \tag{4.5}$$

And we can obtain the normalized second order derivative operator of exponential filter:

$$fL''(x) = f_1(x) + f_2(x) - 2d(x) \tag{4.6}$$

The first and the second order directional derivative operators for symmetric exponential filter can be written like this in KHOROS routine:

$$fx(x,y) = fL(y) * (f2(x) - f1(x)) \qquad (4.7)$$

$$fy(x,y) = fL(x) * (f2(y) - f1(y)) \qquad (4.8)$$

$$fxx(x,y) = fL(y) * (f1(x) + f2(x) - 2^*d(x)) \qquad (4.9)$$

$$fyy(x,y) = fL(x) * (f1(y) + f2(y) - 2^*d(y)) \qquad (4.10)$$

We use the recursive algorithm, that is available in KHOROS, to implement the above directional derivative operators of symmetric exponential filter in an image.

Supposing $I(x,y)$ is the input image, $I_1(x,y)=I(x,y)\#f_1(x)$ and $I_2(x,y)=I(x,y)\#f2(x)$, we have the recursive algorithm:

$$I_1(x,y) = I_1(x-1,y) + a_0^*(I(x,y) - I_1(x-1,y)) \qquad (4.11)$$

$$I_2(x,y) = I_2(x+1,y) + a_0^*(I(x,y) - I_2(x+1,y) \qquad (4.12)$$

From the Equations (4.1), (4.4), (4.7), (4.8) and (4.9), the band-limited first and second directional derivative of input image can be calculated by the recursive algorithm f_1 and f_2 as follows

$$Ix(x,y)=I(x,y)\#f_1(y)\#f2(y)\#(f2(x)-f1(x)) \qquad (4.13)$$

$$Ixx(x,y)=I(x,y)\#f1(y)\#f2(y)\#(f2(x)+f1(x))-2^*I(x,y)\#f1(y)\#f2(y) \qquad (4.14)$$

$$Iy(x,y) = I(x,y)\#f1(x)\#f2(x)\#(f2(y)-f1(y)) \qquad (4.15)$$

$$Iyy(x,y) = I(x,y)\#f1(x)\#f2(x)\#(f2(y)+f1(y))-2^*I(x,y)\#f1(x)\#f2(x) \qquad (4.16)$$

With this algorithm, we can calculate at the same time the band-limited first and second directional derivative Ix and Ixx (or Iy and Iyy) of input image.

The maxima of gradient or zeros of the second order directional derivative along the gradient are the natural definition of intensity edges. Zeros of the Laplacian are only extensively used for their computational convenience. However, we must stress here that the zero crossing of the Laplacian are not always coincided with the maxima of gradient, for example, the zeros of the Laplacien are farther apart than the maxima of gradient for circularity symmetric patterns, this lack of localization by Laplacien can also be seen in the fact that zeros of Laplacien "swing wide" of corners. Therefore, it had better to detect the edges by maxima of gradients or zeros of the second directional derivative along the gradient. So in this work, I present two methods for edge detection, one uses maxima of gradient, another uses the zero crossing of second order directional derivative along the gradient, both by using the differential operators of the exponential filter.

1). Edges from the maxima of gradient

Using the first order derivative operator of the exponential filter (see Section 4.2.2), the two band-limited first order derivatives, Ix and Iy, can be calculated, and the gradient vector can therefore be determined approximately for every point in the image. The gradient magnitude image is then non-maxima suppressed in the gradient direction and threshold with hysterics, i.e. if the entire segment of the contour lies above a low threshold T1, and at least one part of the segment is above a high threshold T2, that contour is output. The non-maxima suppression scheme requires three points, one of which will be the current point, and the other two should be estimated from the gradient magnitude at points displaced from the current point by vector normal to the edge direction. Figure 4.5 shows the result of this method.

2). Edges from the zero-crossings of the second order directional derivative along the gradient direction

Because edges detected from local gradient maxima can not be a pixel width (less precision of localization), we propose another method which detect the edges from the zeros crossing of the second directional derivative along the gradient direction.

We can calculate I_x, I_y, I_{xx} and I_{yy} by using the method shown above, and therefore obtain approximately the gradient vector and the second order directional derivative along the gradient direction for every point in image. We extract at first the zero crossing of second order directional derivative along the gradient direction on which the gradient magnitude must be above a low threshold, so an edge image is obtained. To this image, the entire segment of the contour will kept, if the gradient magnitude on at least one part of this contour is above a high threshold.

From Figure 4.6 , we can see the edges detected by this method are less noisy and with a much better precision in terms of localization than that shown in Figure 4.5.

Filtering is a problem of estimation from noisy signal, and edge detection is a problem of estimating the positions of maximal local signal changes. Up to now, many works have been done for edge detection in image processing, and different filters are proposed, for example, Gaussian filter, Canny filter, Deriche filter and the exponential filter that is used in this thesis. The exponential filter is chosen to use here because of its good performance listed below:

1) Precision of edge localization

According to Castan [12], we can calculate the average localization error for Gaussian filter, Canny filter, Deriche filter and the exponential filter, denoted by xeG, xeC, xeD, and xeE, respectvely,

xeG = (4*(2*e*3.14)**0.5)/a

xeC = 0.81/a

xeD = 4*exp(-1)/a

xeE = 0

i.e. xeG > xeD > xeC > xeE = 0

So, we can see that the exponential filter localizes edge points with the best precision among these four filters.

2) Signal/Noise ratio on the edge point detected

The signal/noise ratio for the Gaussien filter, Canny filter, Deriche filter and the exponential filter, denoted by snrG, snrC, snrD and snrE, respectively, are:

snrG = 2*s*exp(-32*s) / ((3.14)**0.5

snrC = 0.39/a

snrD = 0.64/a

snrE = 1/a

i.e. snrE > snrD > snrC > snrG

Then, we see that the exponential filter has the best noise eliminating effect among the above four.

According to the analysis results above, the exponential filter is superior to the others at the two principal aspects of the performance of filters.
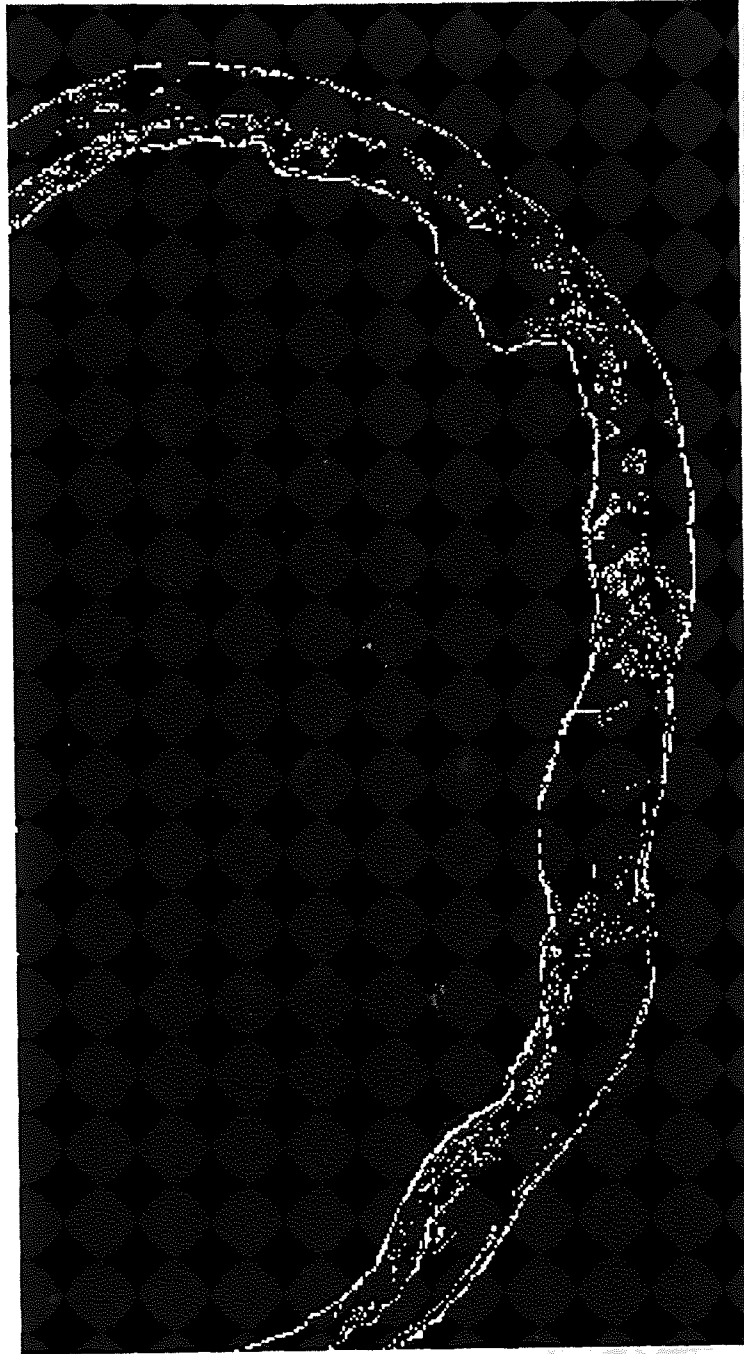
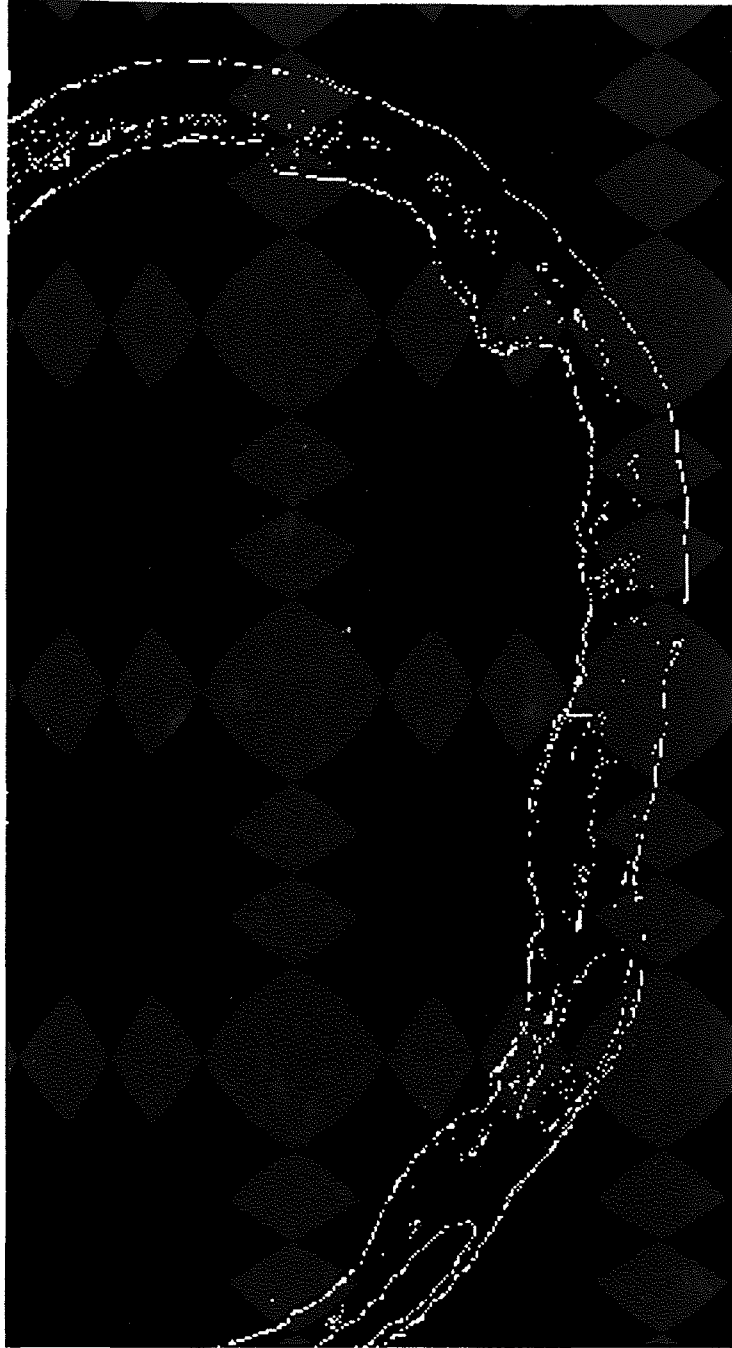Figure 4.5 Edges of the microvessel by using the method of maxima of gradient

Figure 4.6 Edges of the microvessel by using the method of zero-
crossing of second directional derivative along the gradient direction

4.3.2 Snakes Implementation

Kass et al. approximate derivatives in Equation (3.3) with finite differences [4]. If $v_i=(x_i,y_i)$ is a point on the contour, the following approximations are used:

$$|v_s|^2 = |\frac{dv_i}{ds}|^2 = |v_i-v_{i-1}|^2 = (x_i - x_{i-1})^2 + (y_i - y_{i-1})^2$$

$$= E_{cont} \tag{4.17}$$

and

$$|v_{ss}|^2 = |v_{i-1} - 2v_i + v_{i+1}|^2 = (x_{i-1} - 2x_i + x_{i+1})^2 + (y_{i-1} - 2y_i + y_{i+1})^2$$

$$= E_{cure} \tag{4.18}$$

where E_{cont} and E_{curv} are the first- and second-order constraints, the distance between two consecutive pixels in x or y direction is set to 1.

The quantity to be minimized in this implementation of Snakes is

$$J(v) = \int_0^1 (E_{spline} + E_{image} + E_{ext})\ ds$$

$$= \int_0^1 (\alpha(s)E_{cont} + \beta(s)E_{curv} + \gamma(s)E_{image} + \delta(s)E_{ext})\ ds. \tag{4.19}$$

Determining an appropriate approximation for the first term in Eq.4.19, the first order term, encounters some difficulties. Using $|v_i - v_{i-1}|^2$ causes the curve to shrink, as this is actually minimizing the distance between neighboring points. It also contributes to the problem of points bunching up on strong portions of the contour. The tendency is for points to always be moved nearer the previous point, which also moves a point farther from the following point. This causes a chain reaction, moving all points toward the previous ones. In observing the behavior of the given algorithms, it became

apparent that a term which encourages even spacing of the points would reflect the desired behavior of the contours more than one which caused shrinking. So an assumption that the points are spaced at unit intervals have been made here. If the points are evenly spaced, then Equation 4.17 should be divided by d^2, where d is the distance between points, and Equation 4.18 by d^4. This is not a major problem since the values of α and β can be chosen to include these factors.

The second term in Equation 4.19 is curvature, that is v_{ss}, the second order term. Discrete approximation of curvature in an accurate and efficient manner is necessary for curvature term. Williams et al. proposed six different approximations of curvature [10]. Since the formulation of the continuity term causes the points to be relatively evenly spaced, the formula: $|v_{i-1} - 2v_i + v_{i+1}|^2$, giving a reasonable estimation of curvature multiplied by a constant is used in my research work. The constant term is not significant since this term, like the continuity term, is normalized by dividing by the largest value in the neighborhood, giving a number from 0 to 1.

The third term in Equation 4.19, E_{image}, is the image force, which is negative gradient magnitude. Gradient magnitude at each point in the image is input as an eight bit integer, with values 0-255. There is a significant difference between a point with gradient magnitude 240, and one having magnitude 255. This is not reflected when the values are normalized by division by 255. Thus, given the magnitude at a point (mag) and the maximum (max) and minimum (min) gradient in each neighborhood, the following quantity

$$(min - mag)/(max - min)$$

is used for the normalized edge strength term. A negative sign is placed prior to gradient magnitude term so that points with large gradient will have small values.

If (max - min) < 5 then min is given the value (max - 5). This prevents large differences in the value of this term from occurring in areas where the gradient magnitude is nearly uniform.

The last term in Equation 4.19 is the external force, which makes the Snake has a more dynamic behavior. The external forces that push the curve to the edges are modified to give more stable results. In Cohen's model [5], the curve behaves like a balloon which is inflated towards edges by an additional force. It is stopped if the edge is strong, or is passed through if the edge is too weak with respect to the inflation force. From an initial oriented curve we add to the previous forces a pressure force pushing outside as if we introduced air inside. This external force can be defined as

$$F = \delta n(s)$$

where $n(s)$ is the normal unitary vector to the curve at point $v(s)$ and δ is the amplitude of this force. If we change the sign of δ, it will have an effect of deflation instead of inflation.

The parameters α, β, γ and δ are used to balance the relative influence of the four terms above. Their relative sizes, rather than absolute sizes, are significant.

In my research work, I chose $\alpha=1$, $\beta=1$, $\delta=1$ and $\gamma=1.2$. These were chosen so that the image gradient will have slightly more importance than either of the continuity terms in determining where points on the contour move and an edge point can stop the inflation force.

4.4 Algorithm

Based on the above implementation, now we get the algorithm below.

****

Algorithm for the Snakes Model

Index arithmetic is modulo n

Initialize α_i, β_i, δ_i to 1, and γ_i to 1.2 for all i

Do

/*loop to move points to new locations*/

For i=0 to n   /*point 0 is first and last one */

E_{min} = BIG

for j=0 to m-1   /*m is the size of neighborhood*/

$E_{cont,j}$ = $|v_{i,j} - v_{i-1,j}|^2$

$E_{curv,j}$ = $|v_{i-1,j} - 2v_{i,j} + v_{i+1,j}|^2$

$E_{image,j}$ = $(I(i-1,j) - I(i,j))^2$ + $(I(i,j-1) - I(i,j))^2$

$E_{ext,j}$ = $1/|v_{i,j} - v_{i-1,j}|^2$

E_j = α_i $E_{cont,j}$ + β_i $E_{curv,j}$ + γ_i $E_{image,j}$ + δ_i E_{ext}

if E_j < E_{min} then

E_{min} = E_j

j_{min} = j

Move point v_i to location jmin

If Jmin is not current location

ptsmoved+ = 1   /*count points moved */

until ptsmoved<THR   /*THR is the threshold used for convergence

****
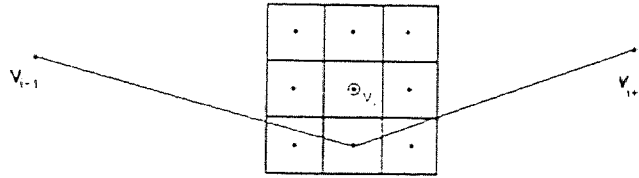
Figure 4.7 Algorithm schema
The energy function is computed at v_i and each of its eight neighbors.
The point before and after it on the contour are used in computing
the continuity constrains. The location having the smallest value
is chosen as the new position of v_i.

Figure 4.7 demonstrates how the algorithm works. The energy function
is computed for the current location of v_i and each of its neighbors. The
location having the smallest value is chosen as the new position of v_i. v_{i-1}
has already been moved to its new position during the current iteration. Its
location is used with that of each of the proposed locations for v_i to compute
the first-order continuity term. The location of v_{i+1} has not yet been moved.
Its location, along with that of v_{i-1}, is used to compute the second-order
constraint for each point in the neighborhood of v_i. For i=0, only old values
are used. For this reason v_0 is processed twice, one as the first point in the list,
and another as the last point. This helps to make its behavior more like that
of the other point.

This algorithm is iterative. At first, an initial contour is put near the
edge by a prior knowledge of the object, see Figure 4.8, then for each contour,
each point in the contour (about 50-60 points spaced a distance of
approximately 4-6 pixels apart) is relocated to the points with the smallest

Figure 4.8 Initial contours of the Snakes

value of energy in the neighborhood. The neighborhood examined at each point consists of the point itself and its eight neighbors, refer to Figure 4.7. Thus the neighborhood size, m was 9. During each iteration, a neighborhood of a point is examined and the point in the neighborhood giving the smallest value for the energy term is chosen as the new location of the point. When a few iterations are done, a local minimum may be reached and the active contour converges to edges. Here a threshold used for determing convergence is a number of points that experience changes during the iteration. That is, when the number of pixels that change their positions during the iteration is less than the predefined threshold, one considers the algorithm converges. In my research work, I choos small, nonzero values, between 2 and 5, as the threshold and they work quite well for our case. Only closed contours are being considered, so all index arithmetic is modulo n. In my work, the several closed boundaries are extracted sequentially. However, in principle, these contours can be extracted parallelly. Figure 4.9 is the final result that we've got after the implementation of the Snakes model.
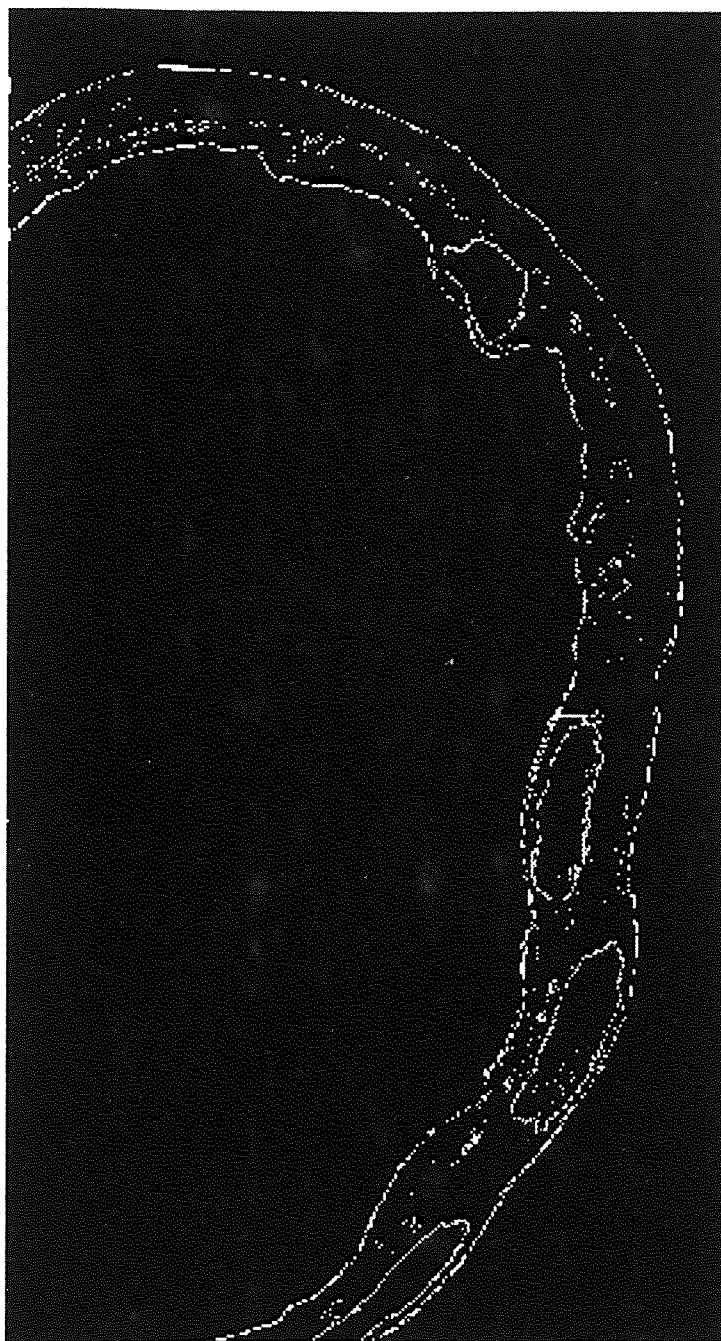
Figure 4.9 Final contours of the Snakes

CHAPTER 5

CONCLUSION AND RECOMMENDATION

Our main goal in this thesis is to extract contours from HVEM image of microvessels. Previous methods to extract contours have generally been based on traditional edge detection operations combined with edge linking or contour-following procedures. Here we do it in an alternative way: we start with a continuous curve model that is localized by the examination of the zero-crossings of the second order directional derivative along the gradient direction according to the Castan local edge detector. Then we draw a simple curve close to the intended contours, (see Figure 4.8). The Snake algorithm is then applied. The action of the image forces and external forces push the initial contour curve the rest of the way. The internal forces serve to impose a piecewise smoothness constraint on the curve. The final position corresponds to the equilibrium reached at the minimum of the model's energy. Figure 4.9 shows the final positions of contours extracted.

Using the Snake model to extract the contour of microvessels from HVEM image provides better results than the conventional contour extraction methods by Liu, described in Chapter 2. Comparing Figure 4.9 with Figure 2.2, we can see the use of the Snakes significantly improves the results. For instance, our algorithm developed here is capable of extracting the compartments of the microvessel such like Endothelium Nucleus and Smooth Muscle Nucleus, which had not been extracted by Liu's method. From Figure 4.9, we can also see that the contours have settled nicely around the edges of the microvessel. This is an indication of the accuracy of localization of edges obtained by using the Snake model.

43

In the field of computer vision, the problem for detection of edges, or other feature, seems to lie on combining local information. However, they may be able to be obtained nicely with a global structure. Snakes [4] provide an elegant way of linking local information to form edges, of providing a prior knowledge about the likely structure of an edge. In this thesis, it is a first time trial to apply the Snake model to HVEM images in order to obtain a contour data file of microvessels. The final result shows that the method is practical and the result is acceptable.

However, our algorithm developed here is not capable of detecting the compartment of Internal Lamina. The problem lies in: a) our algorithm considers only closed contours, but the IL in the original image (see Figure 4.1) that we obtained from HP scanner is not close because of the size limitation of the scanner, b) we only used montage prints with a enlargement of 2500x in the research work so that the digitized image is not clear enough to obtain more information for the IL compartment. Therefore in the future, we can try to extract the boundary of IL by working on larger and finer HVEM images of microvessels that contain complete IL.

Some ideas developed in this paper deserve more attention in future work. First, the idea of initial contour prediction could certainly be more accurate than we have obtained at present. The penalized maximum likelihood algorithm to obtain an initial contour proposed by Liu et al. [3] could be considered. Second, we could use a frequency domain analysis of the active contour algorithm [17]. It can provide interesting insights into the behavior of the algorithm and a fast way of solving closed active contour problems. Finally, an analysis could be conducted to examine how accurate the extracted contours of interest are compared with true contours.

REFERENCES

1. Horn, L., W.S Krajewski, P.K. Paul, M.J. Song and M.J. Sydor. "Computerized 3-D Reconstruction of Small Blood Vessels From High Voltage Electron Microsgraph of Thick Serial Cross Section." *Vascular Endothelium in the Health and Disease,* Plenum Publishing Corporation, 1988.

2. Braverman, M.S., I.M. Braverman. "Three Dimensional Reconstructions of Objects from Serial Sections Using a Microcomputer Graphics System." *J. Investig. Dermatology 86,* 1986, pp. 290-294.

3. Liu, L. , B.G. Schunck and C.R. Meyer. "Optimal Contour Approximation by Deformable Piecewise Cubic Splines." *Proc. of IEEE Int. Workshop on Robust Computer Vision,* Seattle, 1990.

4. Kass, M., A. Witkin, and D. Terzopoulos. "Snakes: Active Contour Models." *Proceedings of First International Conference on Computer Vision,* London, 1987, pp. 259-269.

5. Cohen, L.D.. "Note on Active Contour Models and Balloons." *Image Understanding,* Vol. 52, N2, 1991, pp. 211-218.

6. Rong, J., R. Colloree, J. Coatrieux and C. Toumoulin. "Model-guided Automatic Frame-to-Frame Segmentation in Digital Subtraction Angiography. " *Proc. SPIE Science and Engineering of Medical Imaging Conference,* Vol. 1137, 1989, pp. 31-36.

7. Gwydir, S.H., H.M. Buettner, and S.M. Dunn. "Feature Extraction for Non-Rigid Motion Analysis Using Continuity Spline." *Proceedings of 19th IEEE Annual Northeast Bioengineering Conference,* 1993, pp. 50-51.

8. Cohen, I., L.D. Cohen and N. Agache. "Using Deformable Surfaces to Segment 3-D Images and Infer Differential Structure." *Image Understanding,* Vol. 56, Mo.2 1992, pp. 242-263.

9. Amini, A. A., S. Tehrani and T.E. Weymouth. "Using Dynamic Programming for Minimizing the Energy of Active Contours in the Presence of the Hard Constraints." *Proceedings of Second International Conference on Computer Vision,* 1988, pp. 95-99.

10. Williams, Donna J. and Mubarak Shah. "A Fast Algorithm for Active Contours and Curcature Estimmation" *CVGIP Image Understanding,* Vol. 55, No. 1, January, 1992, pp. 14-26.1

REFERENCES
(Continued)

11. Liu, Y. G.. "Automatic Contour Extraction from HVEM Images of Microvessels." *Master Thesis*, NJIT, 1990.

12. *Khoros User's Manual.* University of New Mexico, 1991.

13. Crimmins, T.R.. "Geometric Filter for Speckle Reduction." *Applied Optics*, vol. 24, No. 10, 1985, pp 1438-1443.

14 Canny, John. "A computational Approach to Edge Detection." *IEEE Transation on Pattern Analysis and Machine Intelligence.* vol. PAMI-8, No. 6, 1986, pp. 679-688.

15. Marr, D., E. Hildreth. "Theory of Edge Detection." *Proc. R. Soc.*, London, 1980, pp. 187-217.

16. Yuille, Alan L., Davvid S. Cohen and Peter W. Hallinan. "Feature Extraction from Faces Using Deformable Templates." *IEEE Int. Workshop on Robust Compuet Vision,* Seattle, Oct. 1990, pp. 104-109.

17. Davatzikos, Chris A., Jerry L. Prince. "Convergence Analysis of The Active Contour Model with Applications to Medical images." *Proc. SPIE Visual Communications and Image Processing*, Vol 1818, 1992, pp. 1244-1255.